Defence Science Journal, Vol. 74, No. 5, September 2024, pp. 682-689, DOI : 10.14429/dsj.74.19437

Radiation Behavior of Synthesized LiTi Ferrite Based Microstrip Antenna in X Band

Dheeraj Kumar[#,*], Naveen Kumar Saxena[$] and Bhoopendra Singh[$]

[#]*Department of Physics, Rajdhani College, University of Delhi - 110 015, India*
[$]*Microwave Lab, Department of Physics, Agra College, Agra - 282 007, India*
[*]*E-mail: kdheeraj_7@yahoo.co.in*

ABSTRACT

The paper comprehensively explores the development, characteristics, and antenna applications of Lithium Titanium (LiTi) ferrite. Utilising a solid-state reaction technique, the study examines the substrate's electrical, magnetic, and structural properties in detail. Additionally, it assesses the far-field radiation patterns of a magnetically-biased LiTi ferrite-based antenna. Key findings point to a noticeable reduction in mutual coupling and radiated power, along with an isotropic redistribution of minor side lobes. Comparative analysis with RT-duroid substrates in X band frequency spectrum highlights the LiTi ferrite-based antenna's remarkable 62.85 % miniaturisation and consistent directivity, along with a superior quality factor. These findings emphasise LiTi ferrite's potential for compact, high-performance applications in demanding environments. LiTi ferrite's advantages in miniaturisation and stability position it for specific applications, despite trade-offs in bandwidth, gain, and impedance compared to RT-duroid substrates.

Keywords: Substituted ferrite; Microstrip antenna; Switchable antenna; Miniaturization; Mutual coupling; X-band

1. INTRODUCTION

Substituted ferrites serve as cornerstone materials in the microwave sector, particularly due to the growing need for high-frequency communication systems. Lithium-substituted ferrites, in particular, demonstrate several benefits when compared to conventional dielectric substrates, notably in microwave antenna deployments. These benefits encompass size miniaturization, low-temperature sintering, high dielectric constants, minimized surface wave excitation, and lower loss characteristics. A distinguishing feature of ferrite-based materials lies in their nonreciprocal properties, as evidenced by a direction-dependent magnetic resonance width (ΔH), rendering them ideal candidates for high-frequency functionalities[1-4]. While prior work has focused on the incorporation of divalent, trivalent, and tetravalent ions in lithium-substituted ferrites,[5-6] along with their potential utility in C and S bands,[7-14] no reports exist on the implications of adding titanium ions (Ti) specifically for X-band deployments. The exploration of enhancing the distinctive nonreciprocal attributes of Li ferrites through Ti doping, particularly for magnetically biased antenna systems, constitutes the core of this research. Focused on a 1×4 rectangular patch antenna array, the study delves into the utilisation of LiTi ferrite substrates with magnetic biasing to address mutual coupling effects. This study advances the understanding of lithium-substituted ferrites and highlights the potential of LiTi ferrites for X-band deployments. The introduction of titanium ions adds a novel dimension to the nonreciprocal properties of these materials, positioning them as promising candidates for high-frequency functionalities. Moreover, this work aligns with recent trends in ferrite-based antenna design, including investigations by Mashhadi, *et al.* into ferrite-based wideband circularly polarized microstrip antennas,[15] Bhongale's exploration of Mg-Nd-Cd ferrite as a substrate for X-band microstrip patch antennas,[16] Chen, *et al.* research on a tunable broadband microstrip antenna based on ferrite material,[17] and Bhongale, *et al.* study on the effect of Nd^{3+} substitution on structural and magnetic properties of Mg–Cd ferrites[18]. Additionally, Asif[19], *et al.* synthesis and characterization of Tb-doped Ni–Zn nano ferrites for dual-band MIMO antennas provide valuable insights[19]. These recent studies collectively reinforce and complement the findings, underscoring the significance of ferrite-based materials in advancing antenna technologies. The research presented here substantively contributes to this evolving landscape and lays a foundation for further exploration in the realm of ferrite-enhanced antenna systems.

2. METHODOLOGY

LiTi ferrite was formulated at ambient conditions through the Solid-State Reaction Technique (SSRT)[20]. The resultant material displayed a magnetization ($4\pi M_s$) of 2200 Gauss with a variance of ±5 % and a Curie temperature (T_c) of 500 K, also with a variance of ±5 %. Chemical ingredients were selected based on the formula $Li_{0.63}Mn_{0.1}Ti_{0.26}Fe_{2.01}O_4$. High-purity chemicals were amalgamated with deionized water in a polypropylene vessel in adherence to stoichiometric ratios. To control Fe^{2+} ion generation and impact magnetostription, Mn^{3+} ions were integrated into the base composition. Bismuth

Received : 04 September 2023, Revised : 23 January 2024
Accepted : 03 February 2024, Online published : 19 September 2024

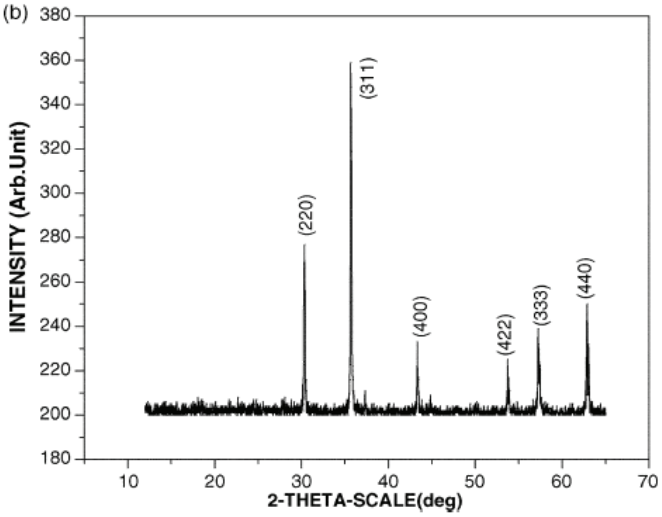

Figure 1. XRD patterns of the prepared ferrite.

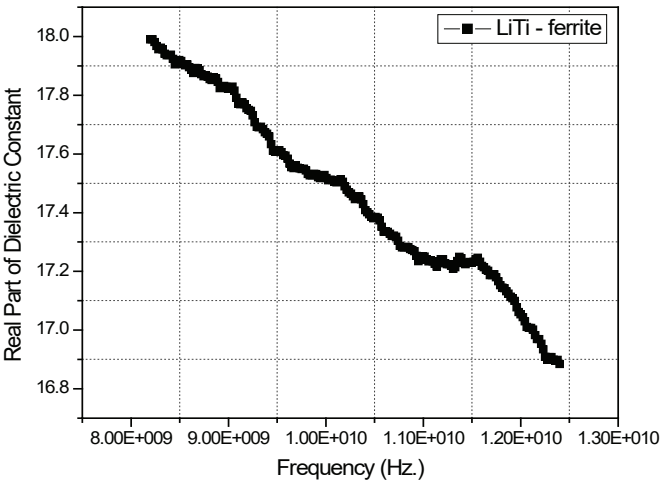

Figure 2. Dielectric constant of material.

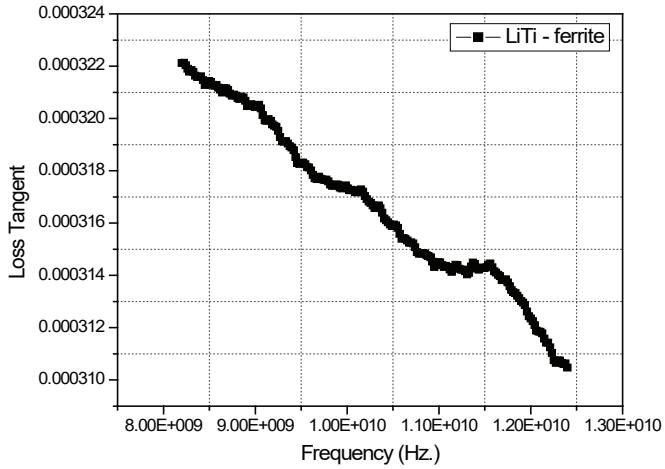

Figure 3. Loss tangent of material.

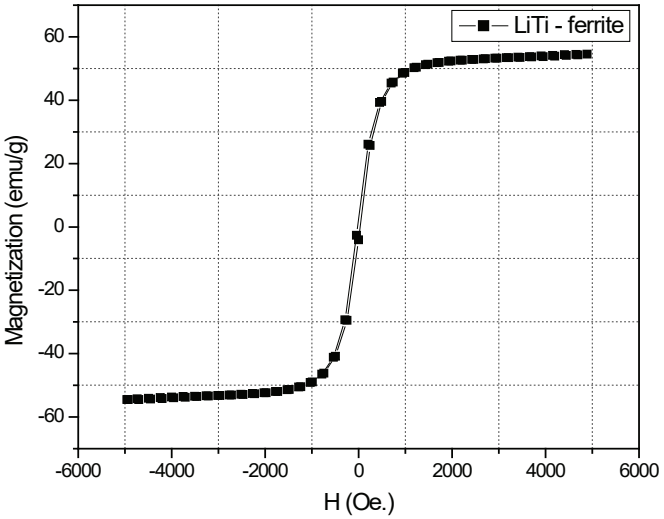

Figure 4. VSM data of dielectric constant.

trioxide (Bi_2O_3) was included as a sintering enhancer at a concentration of 0.25 wt % to counteract Lithia formation under elevated thermal conditions[21]. The premixed powder underwent an initial sintering stage in a box-type furnace at an approximate temperature of 750 °C for a four-hour duration. Post sintering, the material was sieved and molded into disk and toroidal geometries employing specified dies and a hydraulic press exerting a force of 10 ton/cm^2. The sintered samples were further machined, fine-tuned, and polished to achieve required dimensions and forms. X-ray Diffraction (XRD) analyses were carried out to corroborate the single-phase spinel structure of the samples, as depicted in Fig. 1. The sample's microstructural attributes were scrutinised using Scanning Electron Microscopy (SEM). For the purpose of dielectric property evaluation, rectangular pellets with dimensions of 25 mm ×13 mm ×7 mm were selected. These measurements spanned the frequency range of 8-12 GHz and were conducted with an E8263B Agilent Technology Vector Network Analyzer (VNA). The real component of the dielectric constant (ε') was computed based on the equation ε' = $Ct/\varepsilon_0 A$, in which 'C' signifies the specimen's capacitance, 't' its thickness, and 'A' its surface area, with 'ε_0' denoting the permittivity of free space (8.854 x 10^{-12} F/m). Density evaluations were performed through an Archimedes' principle-based experimental setup. Hysteresis loop metrics, including remanence and coercive force, were ascertained via a B-H loop assembly utilizing a toroidal sample coil at a frequency of 50 Hz. LiTi ferrite samples' Curie temperature was gauged employing a gravity-effect-based experiment conducted in-house. The electrical and magnetic attributes of the LiTi ferrite substrate were empirically determined and are summarised in

Table 1. The physical properties of LiTi ferrite substrate

LiTi ferrite characteristics	Values
Magnetic Saturation ($4\pi M_s$)	2200 Gauss
Curie Temperature (T_c)	500^o K
Density (ρ)	4.3 grams/cm^3
Remanence	0.91
Coercivity	2.2
Dielectric Constant (ε)	17.5
Resonance Line Width (ΔH)	520 Oersteds
Loss Tangent (tan δ)	< 0.0005

Table 1. Experimental analysis of the dielectric constant and loss tangent were executed and graphically represented in Fig. 2 and Fig. 3. A Vibrating Sample Magnetometer (VSM) was employed to quantify the magnetic characteristics of the formulated samples, as illustrated in Fi. 4.

3. ANTENNA STRUCTURE

As illustrated in Figure 5, the antenna's structural outline comprises a single patch embedded on a LiTi ferrite substrate. The substrate's physical dimensions are characterized by a thickness ('h'), length ('L'), and width ('W'). The dielectric constant and saturation magnetization of this substrate are noted to be 17.5 and 2200 Gauss, respectively. Given the fragile nature of these substrates, stripline feed methodology is adopted as preferable to other feed techniques. Figure 6 reveals the layout and coordinate framework of a linear array configured with four rectangular patch elements. These are serially linked by a high-impedance transmission line, and power is supplied at the first element[22-24]. One of the advantages of adopting a series-fed array configuration is the bandwidth extension, which scales with the number of elements, albeit up to a limit dictated by the operational frequency and dielectric medium.

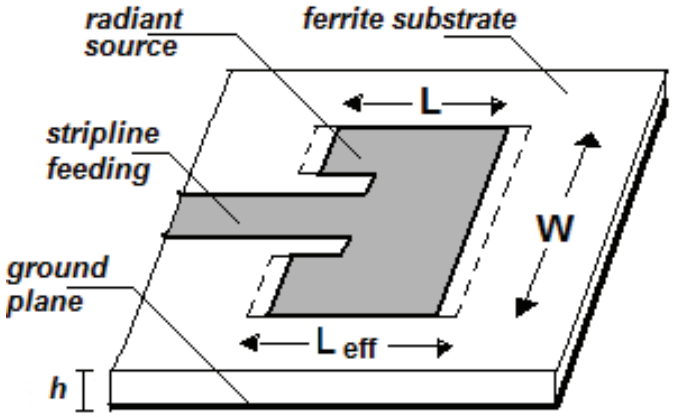

Figure 5. Geometry of microstrip rectangular patch antenna.

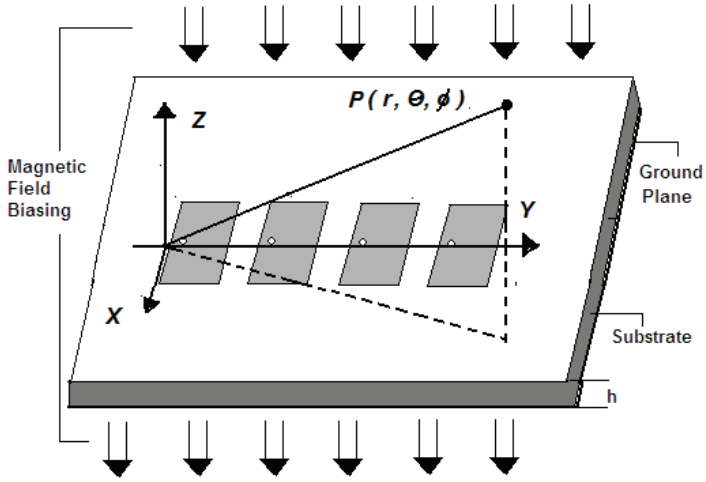

Figure 6. Geometry of li near array of microstrip rectangular patch antennas.

4. THEORETICAL FRAMEWORK

It's well-established that an individual element's behavior within an array is subject to influence from neighboring elements. Element spacing is another contributing factor to such performance alterations. This interaction is commonly referred to as mutual coupling. In the architecture of antenna arrays, factors such as polarisation, beamwidth, and input impedance for an isolated element can experience modifications due to the presence of adjacent elements. Additionally, because mutual coupling fluctuates with the scan angle, it leads to variations in input impedance as the array scans, subsequently impacting its operational efficiency. The relative alignment of these elements also plays a role in this mutual coupling effect. Consequently, when designing and operating array antennas, the implications of mutual coupling should be carefully considered[22-24]. The magnitude of this phenomenon is typically expressed by the numerical value of $|S_{12}|$.

$$|S_{12}| = \frac{2\cos\left(\frac{\pi d}{2}\right)}{\left[\left(1+\cos\left(\frac{\pi d}{2}\right)\right)^2 + \left(\frac{0.882d}{h}\right)^2\right]^{\frac{1}{2}}} \quad (1)$$

For uncoupled case, the far field E-plane ($\theta = 90^o$) radiation pattern can be described as follows:

$$E_{\theta t} = E_{\varphi s}(AF) \quad (2)$$

where,

$$E_{\phi s} = -j2V_0 a k_0 \frac{e^{-jk_0 r}}{4\pi r}\left(\frac{\sin(\frac{k_0 h\cos\phi}{2})}{\frac{k_0 h\cos\phi}{2}}\right)\times\cos(\frac{k_0 h\cos\phi}{2}) \quad (3)$$

$$AF = 4\cos\left(k_0 d_x\cos\theta + b_x\right)\cos\left(\frac{k_0 d_x\cos\theta + b_x}{2}\right) \quad (4)$$

In the current antenna configuration under study, accounting for mutual coupling, the radiation pattern can be characterised as follows:

$$E_{\theta t} = E_{\varphi 1}(1-\Gamma_1) + E_{\varphi 2}(1-\Gamma_2) + E_{\varphi 3}(1-\Gamma_3) + E_{\varphi 4}(1-\Gamma_4) \quad (5)$$

$$|E_{\theta t}| = E_{\phi s}\left[\begin{array}{l}(1-\tilde{A}_1)\left(\cos(\frac{k_o d_x\cos\phi+\beta_x}{2})\right)^{\frac{1}{2}} + \\ +(1-\tilde{A}_3)\left(\cos(\frac{k_o d_x\cos\phi+\beta_x}{2})\right)^{\frac{1}{2}} \\ (1-\tilde{A}_2)\left(\sin(\frac{k_o d_x\cos\phi+\beta_x}{2})\right)^{\frac{1}{2}} \\ +(1-\tilde{A}_4)\left(\sin(\frac{k_o d_x\cos\phi+\beta_x}{2})\right)^{\frac{1}{2}}\end{array}\right] \quad (6)$$

In this specific array arrangement, $E_{\varphi 1}$, $E_{\varphi 2}$, $E_{\varphi 3}$ and $E_{\varphi 4}$ represent the radiation patterns of the respective array elements. Similarly, Γ_1, Γ_2, Γ_3 and Γ_4 signify the reflection coefficients corresponding to these array elements. These reflection coefficients are defined as follows:

$$\left|\tilde{A}_i\right| = \left|\frac{Z_{in} - Z_{fl}}{Z_{in} + Z_{fl}}\right| \tag{7}$$

In this configuration, Z_{in} represents the input impedance of each individual element within the array, while Z_{fl} indicates the impedance of the interconnecting transmission line between these elements. To further analyze the array's behavior, each element can be modeled as a rectangular microstrip patch with ports located along its non-resonant sides. The impedance matrix, or Z-matrix, can then be formulated following the methodology presented in reference 22.

$$Z_{ij} = -j\omega\mu_0 h \sum mn \left[\left(\frac{\phi_{mn}(x_i, y_i)\phi_{mn}(x_j, y_j)}{k^2 - k^2_{mn}} \right) \times \left(\frac{\sin(\frac{m\pi Wf}{2a})}{\frac{m\pi Wf}{2a}} \right) \right] \tag{8}$$

$$\phi_{mn}(x_i, y_i) = \sqrt{\frac{\varepsilon_{0m}\varepsilon_{0n}}{ab}} \cos\left(\frac{m\pi x}{a}\right) \cos\left(\frac{n\pi y}{b}\right) \tag{9}$$

where,

$$k^2 = \varepsilon_r \left(1 - j\tan\delta\right) \frac{\omega^2}{c^2} \tag{10}$$

$$k^2_{mn} = \left(\frac{m\pi}{a^2}\right)\left(\frac{n\pi}{b^2}\right) \tag{11}$$

Upon interaction of a normally incident plane wave with a magnetically biased ferrite substrate, two distinct wave types are generated: volume magnetostatic waves and their surface counterparts, also known as surface magnetostatic waves (MSW)[25-30]. The literature indicates that the initiation of MSW within the ferrite material consequently results in the formulation of associated absorption and transmission coefficients[21,25].

$$P = \frac{2\beta_o\varepsilon_r \left(asin2\beta\delta + \beta\sinh\left(2a\delta\right)\right)}{\left[\begin{array}{l} \beta_0{}^2\varepsilon_r{}^2\left(cos^2\beta\delta + \sinh^2 a\delta\right) + \\ \left(\alpha^2 + \beta^2\right)\left(\begin{array}{l}\sin^2\beta\delta \\ +\sinh^2 a\delta\end{array}\right) + \\ \beta_o\varepsilon_r \left(asin2\beta\delta + \beta\sinh\left(2a\delta\right)\right) \end{array}\right]} \tag{12}$$

$$T = \frac{8\left(\alpha^2 + \beta^2\right)\beta_0{}^2\varepsilon_r}{\left[\begin{array}{l} \left(4\beta^2\beta_0{}^2\varepsilon_r{}^2 + \left(\alpha^2 + \beta^2 + \beta_0{}^2\varepsilon_r{}^2\right)^2\right)\cosh\left(2a\delta\right) \\ +4\beta\beta_o\varepsilon_r\left(\alpha^2 + \beta^2 + \beta_0{}^2\varepsilon_r{}^2\right)\sinh\left(2a\delta\right) \\ -\left(4\beta^2\beta_0{}^2\varepsilon_r{}^2 + \left(\alpha^2 + \beta^2 - \beta_0{}^2\varepsilon_r{}^2\right)\right)\cosh\left(2\beta\delta\right) \\ +4\alpha\beta_o\varepsilon_r\left(\alpha^2 + \beta^2 - \beta_0{}^2\varepsilon_r{}^2\right)\sinh\left(2\beta\delta\right) \end{array}\right]} \tag{13}$$

where,

$$\alpha = \beta_0\sqrt{\frac{\varepsilon_r}{2}}\sqrt{\left[\sqrt{\left(\mu'^2 + \mu''^2\right)} - \mu'\right]} \tag{14}$$

$$\beta = \beta_0\sqrt{\frac{\varepsilon_r}{2}}\sqrt{\left[\sqrt{\left(\mu'^2 + \mu''^2\right)} + \mu'\right]} \tag{15}$$

$$\mu' = 1 + \chi' \tag{16}$$

$$\mu'' = \chi'' \tag{17}$$

$$\chi' = \frac{\omega_m T\left(\omega_0 + \omega\right)}{\left(\omega_0 - \omega\right)^2 T^2 + 1} \tag{18}$$

$$\chi'' = \frac{\omega_m T}{\left(\omega_0 - \omega\right)^2 T^2 + 1} \tag{19}$$

$$T = \frac{2}{\gamma \times \Delta H} \tag{20}$$

$$\beta_0 = \frac{\omega}{c} \tag{21}$$

In the context of a ferrite substrate, both surface and volume magnetostatic waves (MSW) propagate in a direction that is perpendicular to the externally applied magnetic field.

For Volume MSW, the boundary conditions of the frequency band are:

$$\mu_0\gamma H < \omega < \mu_0\gamma\sqrt{H\left(H + M_0\right)} \tag{22}$$

Surface MSW, the boundary conditions of the frequency band are:

$$\mu_0\gamma\sqrt{H\left(H + M_0\right)} \le \omega \le \mu_0\gamma H\left(H + \frac{M_0}{2}\right) \tag{23}$$

Quasi TEM mode of wave: Under applied magnetic field strength the vector permeability tensor for a ferrite is given by[3]

$$[\bar{\mu}] = \begin{bmatrix} \mu & jk & 0 \\ -jk & \mu & 0 \\ 0 & 0 & 1 \end{bmatrix} \tag{24}$$

Where, μ and k vary with the applied magnetic field strength. It has been found that for a normal incident plane wave on biased ferrite slab, two types of waves are generated, ordinary and extraordinary. The ordinary wave behaves just like the plane wave moving through a dielectric material and not affected by the magnetic nature of the medium. On the other hand, the extraordinary wave is characterised by TE mode polarization that aligns with the magnetic bias. The propagation constant K_o and K_e for ordinary and extraordinary wave respectively may be given as follows:

$$K_0 = \frac{\omega}{c}\sqrt{\varepsilon_{eff}} \tag{25}$$

$$K_e = \frac{\omega}{c}\sqrt{\varepsilon_{eff} \times \mu_{eff}} \tag{26}$$

where,

$$\mu_{eff} = \frac{\mu^2 - k^2}{\mu} \tag{27}$$

Here, the parameters μ and k are the functions of frequency given by:

$$k = \frac{\omega\omega_m}{\omega_0{}^2 - \omega^2} \tag{28}$$

$$\mu = 1 + \frac{\omega_0 - \omega_m}{\omega_0{}^2 - \omega_m{}^2} \tag{29}$$

where, $\omega_0 = \gamma H_0$, $\omega_m = \gamma 4\pi Ms$, H_0 represents the external bias field, $4\pi M_s$ is the saturation magnetization of the ferrite substrate and γ denotes the gyromagnetic ratio (γ = 2.8 MHz/Oe). Additionally, ε_r, μ_{eff}, c, ω_0 and ω_m stand for the relative

permittivity, effective permeability of the ferrite substrate, velocity of the electromagnetic wave in free space, the precession and forced frequencies, respectively.

When the effective permeability μ_{eff} takes on a negative value, it indicates a decaying wave, even in a lossless medium. The frequency spectrum for which μ_{eff} becomes negative is:

$$\sqrt{\omega_0(\omega_0+\omega_m)} < \omega < (\omega_0+\omega_m) \quad (30)$$

The frequency limits set the range where the ferrite exhibits notable microwave characteristics.

5. ANALYSIS AND INTERPRETATION

The LiTi ferrite substrate's dielectric properties were assessed within the 8-12 GHz frequency band, employing an Agilent Technologies VNA E8263B impedance analyzer. The corresponding plots for the dielectric constant and loss tangent are depicted in Fig. 2 and Fig. 3, respectively. Vibrating Sample Magnetometer (VSM) was employed to examine the magnetic attributes of the samples, with the saturation magnetization ($4\pi M_s$) showcased in Fig. 4. Operating the ferrite in a biased state while adjusting the ferrite layer thickness can amplify power loss, thus augmenting absorption and attenuation factors.

Figures 7 and 8 provide the transmission and absorption coefficients at h = 2 mm and h = 1.65 mm for varying DC magnetic fields. It can be observed in Fig. 7 that the peaks of the transmission coefficient slightly elevate up to 2200 Oe as the thickness grows, taking a notable shift at elevated magnetic fields. Concurrently, the absorption coefficient peaks display minor fluctuations with the increment in substrate thickness, as presented in Fig. 8.

An increase in the inter-patch distance leads to a reduction in mutual coupling, a phenomenon illustrated in Figure 9, where the mutual coupling shows a direct proportionality to the substrate thickness. When the ferrite is in an unbiased or positive effective permeability ($\mu_{eff} > 0$) state, the antenna operates in standard transmission and reception modes. At a $\mu_{eff} < 0$ state, incoming waves transform into quasi-TEM and magnetostatic waves, thereby highly attenuating the incident RF waves.

The dispersion curve for the X-band frequency under a 750 Oe magnetic field is depicted in Fig. 10. This graph reveals that upon magnetization, the propagation constant (K) undergoes frequency-dependent changes. The curve's initial linear portion represents Pozar's quasi-TEM wave, while the remaining part accounts for magnetostatic wave (MSW) and spin wave excitations. Figure 10 also confirms the antenna's switching off state and indicates a cutoff frequency near 5 GHz. The radiation patterns for antenna arrays fabricated on RT-duroid and LiTi ferrite are illustrated in Fig. 11 and Fig. 12, accounting for mutual coupling. Owing to this coupling, RT-duroid-based antennas display collective side lobes in the E-plane radiation pattern. However, magnetically biased ferrite antennas reduce mutual coupling due to the absorption of undesired guided waves. Moreover, minor side lobes undergo isotropic redistribution, resulting in decreased radiation power. The ferrite-based antenna preserves the primary lobe orientation and offers enhanced directivity, in contrast to its RT-duroid counterpart. These characteristics are comprehensively summarised in Table 2.

Table 2. Comparison of characteristics of microstrip rectangular patch array antenna printed on RT-duroid and LiTi-ferrite

Radiation parameters	Values	
	RT-duroid	LiTi-ferrite
Length (L)	0.86 cm	0.27 cm
Width (W)	1.64 cm	0.69 cm
Band width (BW)	6.14 %	2.42 %
Directivity (D)	4.77 dB	4.77 dB
Q. Factor (Q_F)	8.22	12.27
Gain (G)	4.38 dB	1.86 dB
Total Imped. (Z_{in})	255 ohms	1007ohms
HP Beamwidth	E-82^0, H-156^0	E-166^0, H-178^0

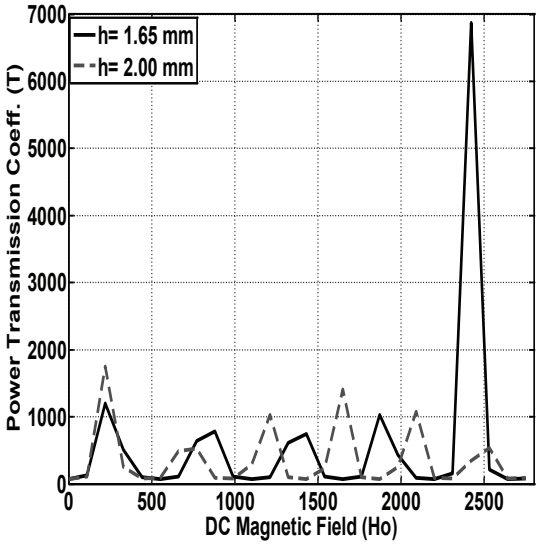

Figure 7. Transmission power coefficient (T) vs DC magnetic field (H_o) at 10 GHz.

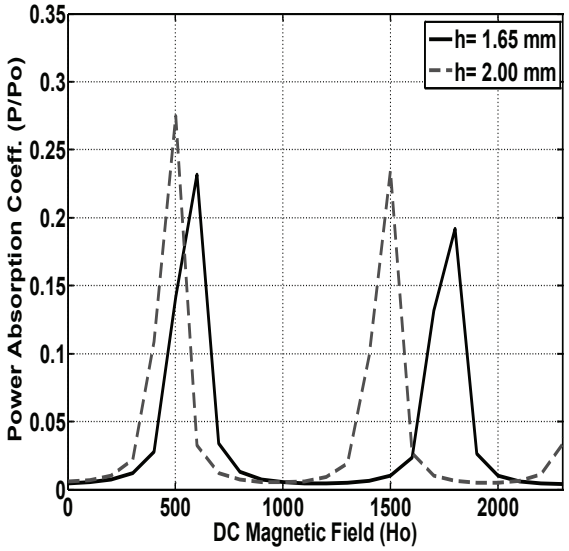

Figure 8. Absorption power coefficient (P) vs DC magnetic field (H_o) at 10 GHz.

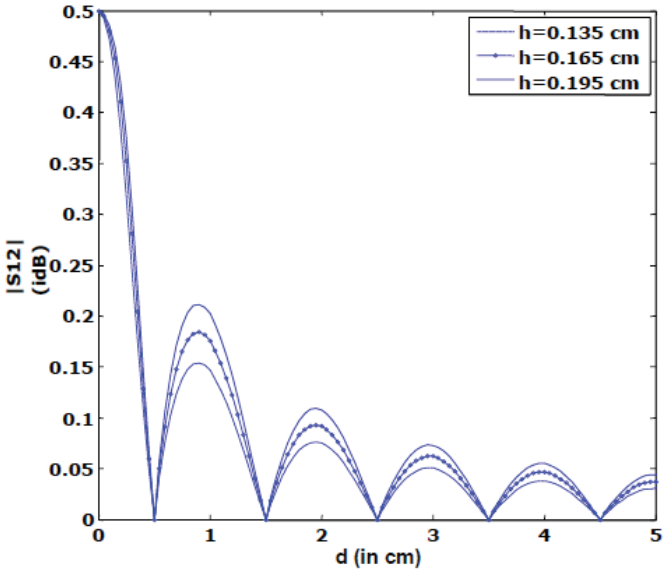

Figure 9. Mutual coupling $|S_{12}|$ vs distance 'd' between array elements.

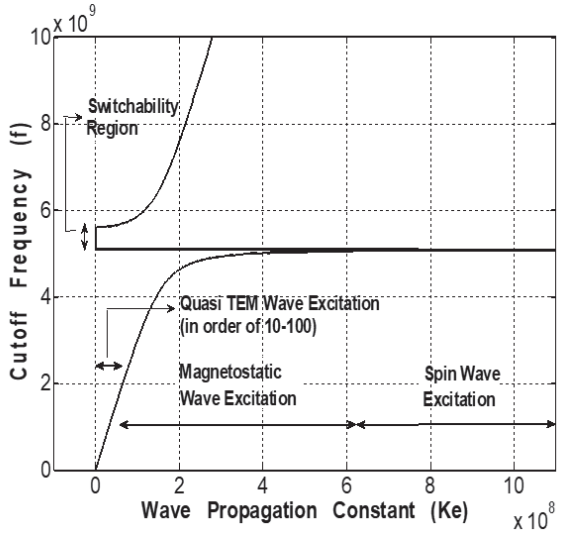

Figure 10. Dispersion curve 'f (Hz) vs. k (rad/m)' of EM-Waves in LiTi for incident plane wave perpendicular to biased radome layer by 750 Oe magnetic field in the X band frequency range.

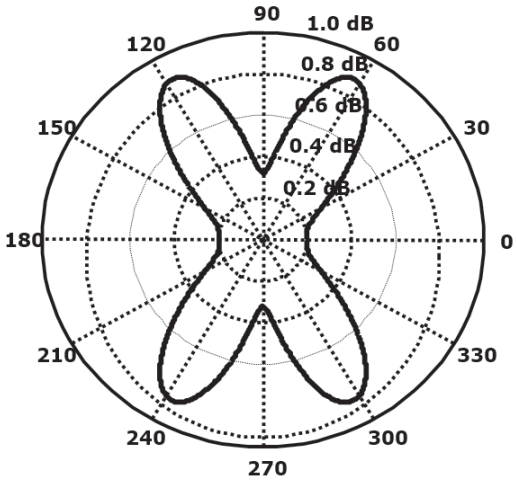

(a)

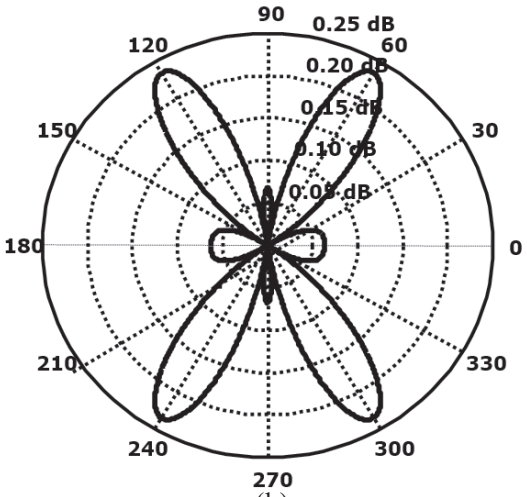

(b)

Figure 11. Radiation pattern of antenna in E-plane ($\varphi = 90^0$) (a) Printed on RT-duroid substrate; (b) Printed on magnetically biased LiTi-ferrite.

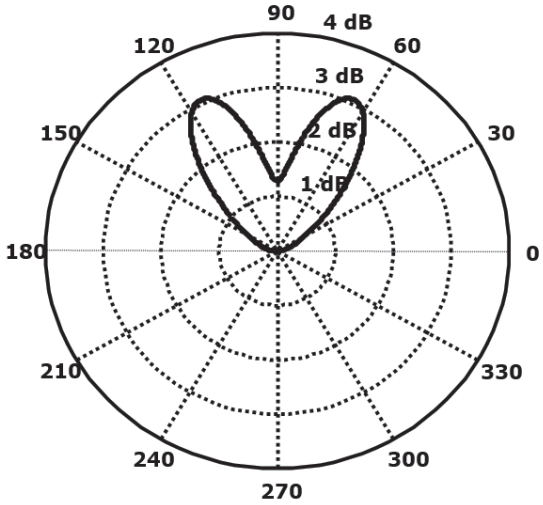

(a)

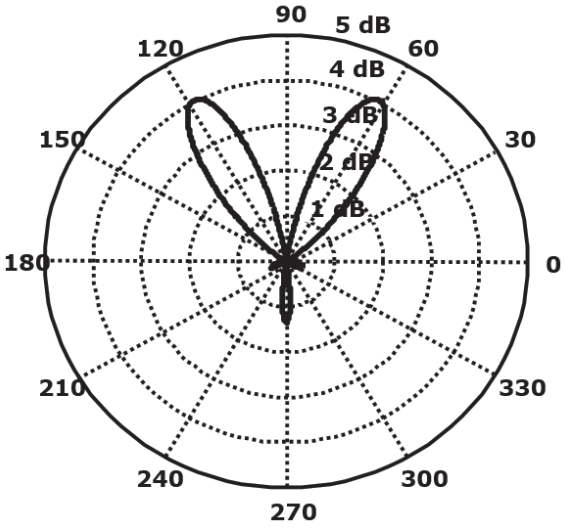

(b)

Figure 12. Radiation pattern in H-plane ($\varphi = 0^0$) (c) printed on RT-duroid substrate. (d) printed on magnetically biased LiTi-ferrite.

6. CONCLUSIONS

This research thoroughly investigates the precise formulation of Li-ferrite incorporated with titanium, characterized by a saturation magnetization of 2200 Gauss. The work also offers an exhaustive exploration of the LiTi ferrite substrate's nonreciprocal attributes when magnetically biased. With its robust saturation magnetization, elevated Curie temperature, and additional essential features, the LiTi ferrite substrate meets the critical specifications needed for microstrip antennas, particularly in demanding operational environments. The magnetic resonance width of the material was studied across various substrate thicknesses to enable antenna tunability and switchability.

A comparative evaluation of the radiation properties between antennas fabricated on RT-duroid and those based on LiTi ferrite was executed within identical frequency spectrums. The findings suggest that the LiTi ferrite-based antenna achieves a significant miniaturization, approximately 62.85 %, when contrasted with its RT-duroid counterpart. This makes it advantageous in scenarios where space conservation is crucial. Additionally, the quality factor for the LiTi ferrite antenna outperforms that of the RT-duroid-based antenna, suggesting its aptness for applications emphasizing miniaturization. Nevertheless, opting for ferrite as the substrate imposes certain limitations, such as reduced bandwidth, directivity, and gain, compared to antennas constructed on RT-duroid substrates. Despite these setbacks in radiation power, the use of LiTi ferrite results in consistent directivity and a superior quality factor, highlighting its potential for specific applications.

REFERENCES

1. Pozar, D.M. Radiation and scattering characteristics of microstrip antenna on normally biased ferrite substrate. *IEEE Trans. Antenna Propag*., 1992, **40**, 1084-1092. doi:10.1109/8.166534.
2. Pozar, D.M. & Sanchez, V. Magnetic tuning of a microstrip antenna on a ferrite substrate. *Electron. Lett*., 1988, **24**, 729-731. doi:10.1049/el:19880491.
3. Tsang, K.K. & Langley, R.J. Design of circular patch antennas on ferrite substrate. *IEE Proc. Microw. Antenna Propag*., 1998, **145**, 49-55. doi:10.1049/ip-map:19981449.
4. Batchelor, J.C. & Langley, R.J. Beam scanning using microstrip line on biased ferrite. *Electron. Lett*., 1997, **33**, 645-646. doi:10.1049/el:19970459.
5. Ravinder, D. Composition dependence of the elastic moduli of mixed lithium-cadmium ferrites. *J. Appl. Phys*., 1994, **75**, 6121-6123. doi.org/10.1063/1.355480.
6. Yang, C. Neutron diffraction study of the magnetism of Li-Zn Ferrites. J. Magn. Magn. Mater., 1992, **116**, 231. doi: 10.1016/0304-8853(92)90167-M.
7. Tsang, K.K. & Langley, R.J. Annular ring microstrip antennas on biased ferrite substrate. *Electron. Lett*., 1994, **30**(16), 1257-1258. doi.org/10.1049/el%3A19940869.
8. Glass, L.H. Ferrite films for microwave and millimeter wave devices. *IEE Proc. Microw. Antenna Propag*., 1988, **76**, 151-158.
9. Das, S.N.; Chowdhury, S.K. & Chatterjee, J.S. Circular microstrip antenna on a ferromagnetic substrate. *IEEE Trans. Antennas Propag*., 1983, **31**, 188-190. doi: 10.1109/TAP.1983.1142997.
10. Yook, J.G. & Katehi, L.P.B. Micromachined microstrip patch antenna with controlled mutual coupling and surface waves. *IEEE Trans. Antennas Propag*., 2001, **49**(9), 1282-1289. doi.org/10.1109/8.947019.
11. Saxena, N.K.; Kumar, N. & Pourush, P.K.S. Radiation characteristics of microstrip rectangular patch antenna fabricated on LiTiMg ferrite substrate. *AEU Int. J. Electron. Commun*., 2015, **69**, 1741-1744. doi: 10.1016/j.aeue.2015.08.005.
12. Bhongale, S.R. Mg-Nd-Cd ferrite as substrate for X-Band microstrip patch antenna. *J. Magn. Magn. Mater.*, 2020, **499**, 165918. doi: 10.1016/j.jmmm.2019.165918.
13. Silva, I.B.T.; D'assunção, A.G. & Oliveira, J.B.L. High-quality nickel ferrite synthesized by a modified sol–gel technique applied as microstrip patch antenna substrate. *J. Electron. Mater.*, 2020, **49**, 4186-4194. doi: 10.1007/s11664-020-08120-y.
14. Vinaykumar, R.; Prakash, S. & Roy, P.K. Synthesis and characterization of Ba2Co2Fe12O22–NiFe2O4 ferrite composites: A useful substrate material in miniaturizing antenna. *J. Mater. Sci. Mater. Electron.*, 2021, **32**, 7330-7339. doi: 10.1007/s10854-021-05443-2.
15. Mashhadi, M.; Komjani, N.; Rejaei, B. & Ghalibafan, J. Ferrite-based wideband circularly polarized microstrip antenna design. *ETRI Journal*, 2019, **41**(3), 289-297. doi: 10.4218/etrij.2017-0291.
16. Bhongale, S. Mg-Nd-Cd ferrite as substrate for X-band microstrip patch antenna. *J. Magnet. Magnetic Mater.*, 2020, **499**, 165918. doi: 10.1016/j.jmmm.2019.165918.
17. Chen, P.; Sun, Z.; Jiang, J.; Li, H. & Li, G. A tunable broadband microstrip antenna based on ferrite material. In Proceedings of the 2020 IEEE 4th Information Technology, Networking, Electronic and Automation Control Conference (ITNEC), Chongqing, China, 2020, pp. 1726-1729. doi:10.1109/ITNEC48623.2020.9084998.
18. Bhongale, S.; Ingawale, H.; Shinde, T. & Vasambekar, P. Effect of Nd3+ substitution on structural and magnetic properties of Mg–Cd ferrites synthesized by microwave sintering technique. *J. Rare Earths*, 2018, **36**(4), 390-397. doi: 10.1016/j.jre.2017.11.003.
19. Asif, R.M.; Aziz, A.; Akhtar, M.N.; Amjad, M. & Khan, M.A. Synthesis and characterization of Tb doped Ni–Zn nano ferrites as substrate material for dual band MIMO antenna. *Physica B: Condensed Matter*, 2023, **653**, 414658. doi: 10.1016/j.physb.2023.414658.

20. Kishan, P.; Sagar, D.R.; Chatterjee, S.N.; Nagpaul, L.K.; Kumar, N. & Laroia, K.K. Optimization of Bi2O3 contents and its role in sintering of lithium ferrite. *Adv. Ceram*., 1985, **16**, 207.
21. Saxena, N.K.; Kumar, N.; Pourush, P.K.S. & Khah, S.K. Study of magnetic properties of substituted LiTiZn-Ferrite for microwave antenna applications. *Optoelectron. Adv. Mater. Rapid Commun.*, 2010, **4**(3), 328-331.
22. Bahl, I.J. & Bhartia, P. Microstrip antennas. Artech House, Norwood, MA, 1980.
23. Bryant, T.G. & Weiss, J.A. Parameters of microstrip transmission lines and of coupled pairs of microstrip lines. *IEEE Trans. Antennas Propag*., 1968, **1**(6), 1021-1027.
doi: 10.1109/TMTT.1968.1126858.
24. James, J.R. & Hall, P.S. Handbook of Microstrip Antenna. Peregrinus, London, 1989.
25. Randhawa, B.S.; Dosanjh, H.S. & Kumar, N. Synthesis of lithium ferrite by precursor and combustion methods: A comparative study. *J. Radioanal. Nucl. Chem.,* 2007, **274**(3), 581-591.
doi: 10.1007/s10967-006-6924-y.
26. Ufimtsev, P. Y.; Ling, R.T. & Scholler, J.D. Transformation of surface waves in homogeneous absorbing layers. *IEEE Trans. Antennas Propag*., 2000, **48**, 214-222.
doi: 10.1109/8.833070.
27. Horsfield, B. & Ball, J.A.R. Surface wave propagation on grounded dielectric slab covered by a high-permittivity material. *IEEE Microw. Guided Wave Lett*., 2000, **10**, 171-173.
doi: 10.1109/75.850367.
28. Lax, B. & Button, K. Microwave ferrite and ferrimagnetics. McGraw-Hill, New York, 1962.
doi:10.1016/0038-1101(63)90107-2.
29. Kabos, P. & Stalmachov, V.S. Magnetostatic waves and their applications. Chapman and Hall, 1994.
doi:10.1007/978-94-011-1246-8.
30. Sodha, M.S. & Srivastav, N.C. Microwave propagation in ferrimagnetics. Plenum Press, 1981.

CONTRIBUTORS

Dr Dheeraj Kumar obtained his PhD degree in Physics. He is working as an Assistant Professor in the Department of Physics at Rajdhani College, University of Delhi, Delhi. His key research interests: Encompass MIMO systems, 5G antenna systems, and terahertz antennas.
Contribution to the current study: Conceptualisation, methodology, software, data curation, reviewed the results and writing original draft preparation.

Dr Naveen Kumar Saxena obtained his PhD degrees in Physics from Dr. B.R. Ambedkar University, Agra. His research interest include: Microstrip antennas, their arrays, ferrite applications for these antennas, and artificial neural network analysis for microstrip antennas and arrays.
Contribution to the current study: Comprehensive literature survey, performing and interpreting all experimental work, as well as simulating and analysing the results.

Dr Bhoopendra Singh obtained his PhD degree in Physics from Dr. B.R. Ambedkar University, Agra. He is working as an Associate Professor in the Department of Physics Agra College, Agra. His expertise lies in microstrip antennas and arrays.
Contribution to the current study: Simulation methodology, reviewed the progress regularly, and consistently provided valuable insights and suggestions.